

AN ULTRAVIOLET-OPTICAL COLOR-METALLICITY RELATION FOR RED CLUMP STARS USING GALEX AND GAIA

STEVEN MOHAMMED

Department of Astronomy, Columbia University, New York, NY 10027

DAVID SCHIMINOVICH

Department of Astronomy, Columbia University, New York, NY 10027

KEITH HAWKINS

Department of Astronomy, Columbia University, New York, NY 10027 and
Department of Astronomy, The University of Texas at Austin, 2515 Speedway Boulevard Stop C1400, Austin, TX 78712

BENJAMIN JOHNSON

Harvard-Smithsonian Center for Astrophysics, Cambridge, MA 02138

DUN WANG

Center for Cosmology and Particle Physics, Department of Physics, New York University, New York, NY 10003

DAVID W. HOGG

Center for Cosmology and Particle Physics, Department of Physics, New York University, New York, NY 10003
Draft version May 10, 2018

ABSTRACT

Although core helium-burning red clump (RC) stars are faint at ultraviolet wavelengths, their ultraviolet-optical color is a unique and accessible probe of their physical properties. Using data from the GALEX All Sky Imaging Survey, Gaia Data Release 2 and the SDSS APOGEE DR14 survey, we find that spectroscopic metallicity is strongly correlated with the location of an RC star in the UV-optical color magnitude diagram. The RC has a wide spread in $(\text{NUV} - G)_0$ color, over 4 magnitudes, compared to a 0.7-magnitude range in $(G_{BP} - G_{RP})_0$. We propose a photometric, dust-corrected, ultraviolet-optical $(\text{NUV} - G)_0$ color-metallicity $[\text{Fe}/\text{H}]$ relation using a sample of 5,175 RC stars from APOGEE. We show that this relation has a scatter of 0.28 dex and is easier to obtain for large, wide-field samples than spectroscopic metallicities. Importantly, the effect may be comparable to the spread in RC color attributed to extinction in other studies.

Subject headings: catalogs, ultraviolet: stars, stars: evolution, Galaxy: general

1. INTRODUCTION

The Milky Way is host to a variety of stars spanning the entire stellar lifetime range. Average stars like our Sun eventually become red giants, some of which populate a prominent feature in color-magnitude diagrams (CMDs) called the red clump (RC) consisting of low-mass, metal-rich stars in the core helium-burning stage of stellar evolution. A sizable fraction of Solar neighborhood giants observed with Hipparcos are RC candidates (60%, Girardi 2016). Metallicities for these stars are readily available from surveys such as APOGEE. The metallicity of RC stars can be used to understand the star formation history and ages of stars in the Milky Way and inform stellar evolutionary models of RC, red giant and horizontal branch stars (Girardi 2016).

With the release of Gaia DR2 (Gaia Collaboration et al. 2018a), the Milky Way can now be probed to greater depths than ever before. The Gaia DR2 release presents parallax measurements for over 1 billion

stars, which provide crucial distance information and G-band measurements to allow construction of the CMD of the Milky Way field population. We combine NUV-band data from the GALEX All Sky Imaging Survey (GAIS, Martin et al. 2005) with Gaia and a catalog of RC stars from APOGEE DR14 (Ting et al. 2018). RC stars are very faint in NUV and should separate clearly from the main sequence. As RC stars have not been extensively probed in UV, this study has the potential to strengthen our understanding the relation between UV-optical colors and the physical properties of stars in this core helium-burning stage. In this paper, we focus on a $(\text{NUV} - G)_0$ color-metallicity relation and show how it compares to a similar color-metallicity relation derived using optical colors. Finally, we also discuss how this relation compares to predictions from stellar evolutionary model tracks, using the MIST code (Dotter 2016, Choi et al. 2016, Paxton et al. 2011, Paxton et al. 2013, Paxton et al. 2015).

2. OBSERVATIONS

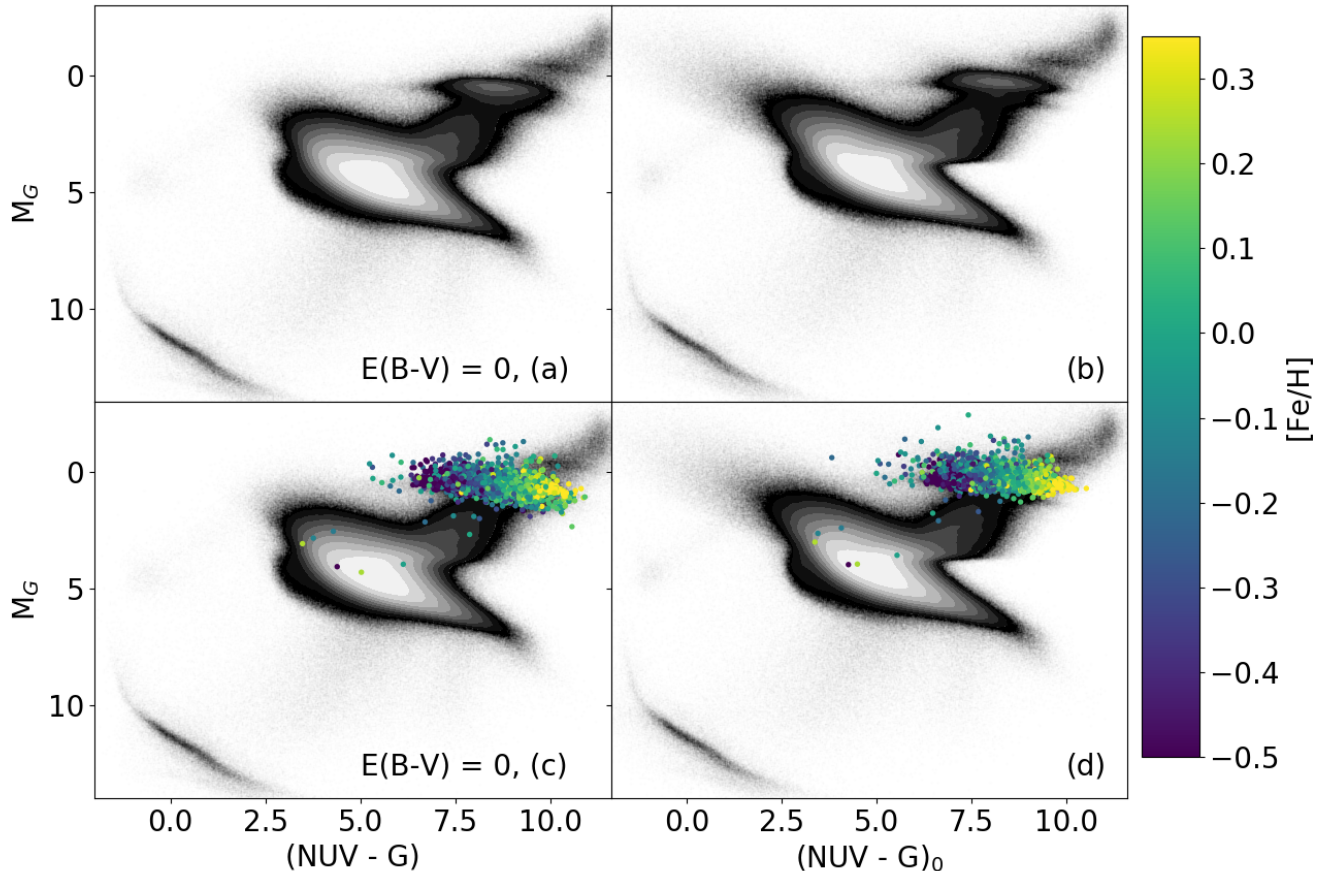


FIG. 1.— M_G vs $(\text{NUV} - G)_0$ distribution for the full parallax-selected (< 3.5 kpc) GAIS-Gaia catalog (top panels) with matches with RC stars shown (bottom panels). The left panels show the CMD without a Galactic extinction correction and the right panels apply a correction as described in the text. The main locus at the center of each panel shows the main sequence. The RC stars are overlaid and colored by $[\text{Fe}/\text{H}]$. There is a clear trend of metallicity with $\text{NUV} - G$ color in both cases. $[\text{Fe}/\text{H}]$ from APOGEE DR14.

2.1. Red Clump data

We build a sample of 5,175 RC stars from Ting et al. 2018 which is constructed using data from the APOGEE (Apache Point Observatory Galactic Evolution Experiment, Majewski et al. 2017) and LAMOST (Large Sky Area Multi-Object Fibre Spectroscopic Telescope, Xiang et al. 2017) surveys. Ting et al. 2018 build a RC sample of 92,249 Milky Way stars from APOGEE DR14 and LAMOST DR3 data with $\sim 3\%$ contamination from red giant stars. For our analysis we only used the pristine RC sample obtained from APOGEE spectra. From its high signal-to-noise, near-infrared ($1.51\text{-}1.70 \mu\text{m}$) spectra, derived parameters such as metallicities, T_{eff} , $\log g$ parameters are available, as well as abundances for many elements. APOGEE elemental abundances are typically accurate to 0.2 dex over the metallicity range considered here (García Pérez et al. 2016).

2.2. GAIS and Gaia DR2

The GALEX All Sky Imaging Survey (GAIS) contains NUV data for millions of objects across the entire sky. Gaia DR2 provides Gaia G , G_{BP} , and G_{RP} magnitudes and parallaxes that can be used to obtain distance information. The errors in G , G_{BP} , and G_{RP} are of the order of millimagnitudes. We apply a small error-dependent correction to the Gaia parallaxes (Lutz & Kelker 1973,

Oudmaijer et al. 1998). We then invert the parallax to get a distance. To cross-match these data we use the astropy (Astropy Collaboration et al. 2013) function *search_around_sky* with a search radius of 3 arcseconds. In total we utilize coverage in GALEX NUV, Gaia G , G_{BP} , G_{RP} and the relevant APOGEE footprint.

Galactic extinction plays a much larger role for the NUV than the other bands (Cardelli et al. 1989) and will have a nontrivial effect on the location of objects in a CMD. To account for this reddening we use the 3D dust map from Green et al. 2015, which gives E_{B-V} as a function of distance, in conjunction with Gaia parallax-derived distances to estimate the reddening in the line of sight of each object in this catalog. The $\text{NUV} - G$ color is dust-corrected (indicated by a 0 subscript) using these E_{B-V} values, adopting R_{NUV} from Yuan et al. 2013, and R_G from Jordi et al. 2010 who obtain R_G values between 2.4 and 3.6. For our analysis, the extinction corrections for NUV and G are $\text{NUV}_0 = \text{NUV} - E_{B-V} \times 7.24$ and $G_0 = G - E_{B-V} \times 2.85$. We are restricted to the sky coverage of the Green et al. 2015 map and remove any objects in the GAIS-Gaia catalog that do not overlap with the map.

For the final catalog we make several additional cuts to the data. The final catalog contains objects that have detections in NUV, G , G_{BP} , and G_{RP} , $[\text{Fe}/\text{H}]$

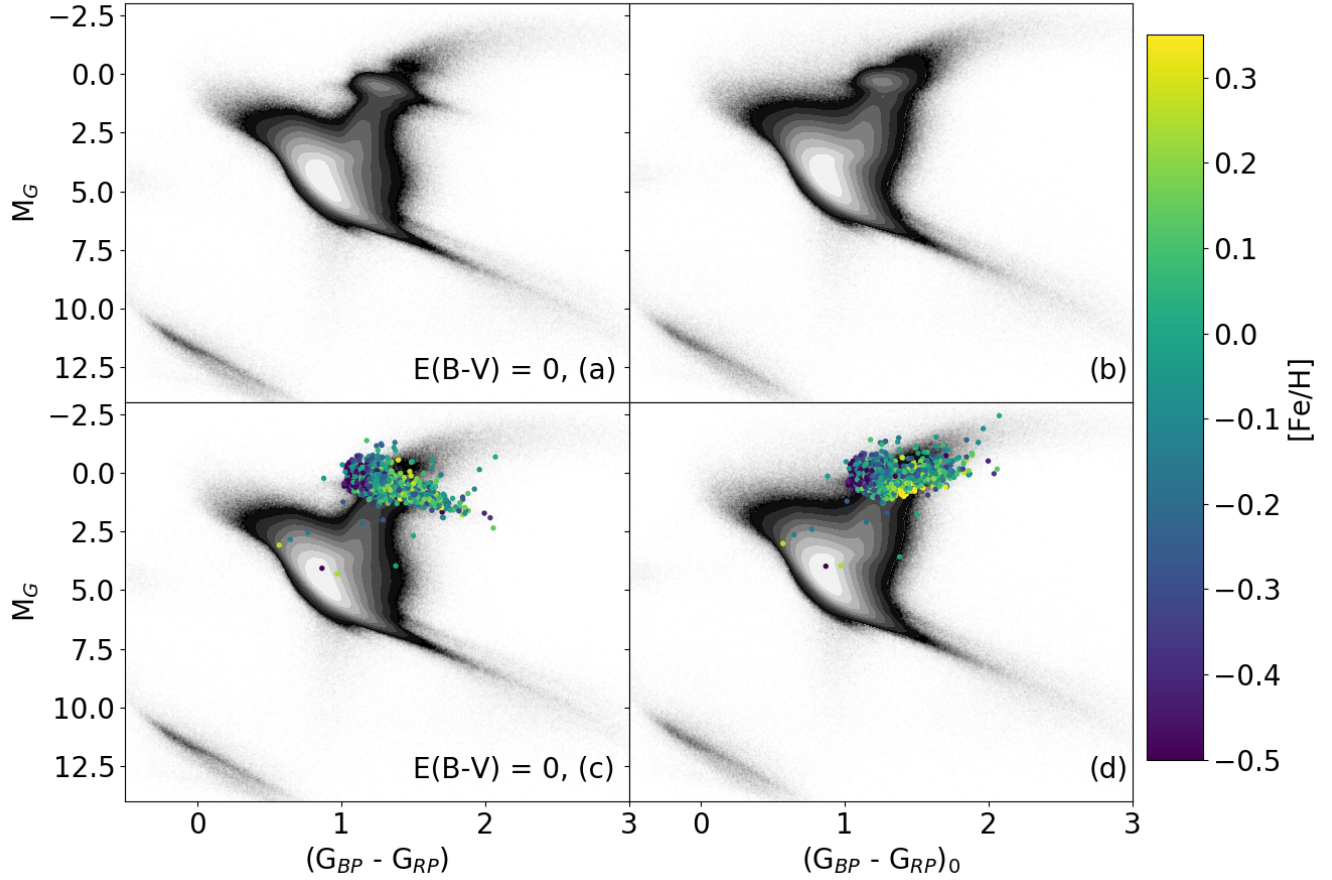


FIG. 2.— M_G vs $G_{BP} - G_{RP}$ distribution for the full GAIS-Gaia catalog (top panels) with matches with RC stars shown (bottom panels). The left panels show the CMD without a Galactic extinction correction and the right panels apply a correction as described in the text.

and T_{eff} measurements, parallax errors less than 10%, $visibility_periods_used > 8$, and distances less than 3500 pc. Additionally, we use the *RC_Pristine* Classification from Ting et al. 2018. We do not require the APOGEE flags to be set to 0 for these objects (65 in total) however the removal of these objects do not impact our results. Our final catalog of GAIS and Gaia objects contains 10,357,542 objects. We cross-match this catalog with the RC catalog and obtain 5,175 matches.

GAIS-Gaia does not appear to be limited to only very blue objects despite the expectation that GALEX would not observe many red stars. There is a large population at the expected position of the RC in the CMD. There are about 91% of objects in the main catalog along the Main Sequence versus 4% of objects in the RC.

3. RESULTS

Figures 1 and 2 show optical and UV-optical CMD histograms for the GAIS-Gaia catalog, using both uncorrected and Galactic extinction-corrected magnitudes. The general shape of the UV-optical CMD is very similar to that of optical: a large main sequence with the red giant branch and RC prominently displayed. The main sequence stretches from $(NUV - G)_0 = 8$ and $M_G = 6$ to $(NUV - G)_0 = 2.5$ and $M_G = 1$, and is where the bulk of the survey matches appear. The secondary locus around $(NUV - G)_0 = 8$ and $M_G = 0$ (Hawkins et al. 2017) is populated by red giants, notably RC stars. The spread of the entire RC in $(NUV - G)_0$ is unlike that

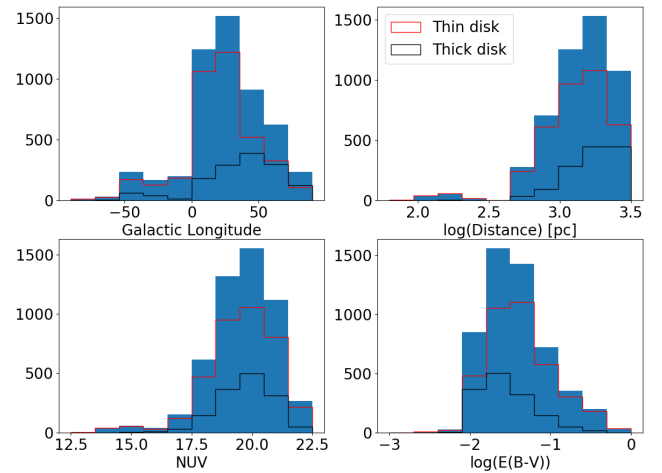


FIG. 3.— Various statistics for our GAIS-Gaia RC sample. The sample is mostly restricted to the upper Galactic plane and at distances greater than 500 pc. We also overplot the thin and thick disk populations discussed further below.

seen in $(G_{BP} - G_{RP})_0$, spreading over 4 magnitudes compared to a spread of 0.7 magnitudes in $(G_{BP} - G_{RP})_0$, as shown in Figure 2. The spread could be due to the age, metallicity, and extinction of the RC stars. As discussed further below, our optical CMD is similar to that of Gaia Collaboration et al. 2018b that shows the appearance of

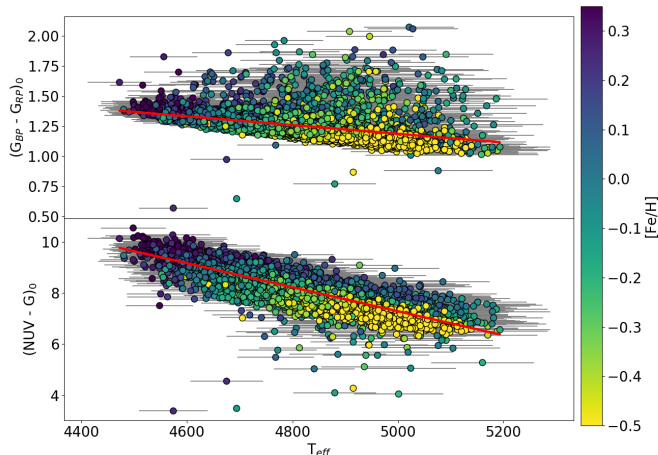


FIG. 4.— T_{eff} from APOGEE vs extinction corrected $(G_{BP} - G_{RP})_0$ and $(NUV - G)_0$ colored by $[\text{Fe}/\text{H}]$ for our RC sample. $(G_{BP} - G_{RP})_0$ shows significant scatter. $(NUV - G)_0$ is more tightly correlated with T_{eff} , although we also identify a subpopulation of very blue outliers.

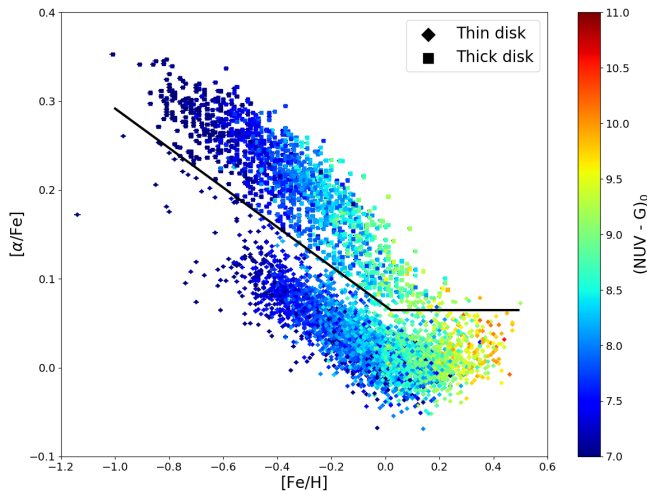


FIG. 5.— $[\alpha/\text{Fe}]$ vs $[\text{Fe}/\text{H}]$ colored by the dust corrected $(NUV - G)_0$ (described in Figure 1). Hawkins et al. 2015 discuss a cartoon depiction of this trend separating the lower branch (thin disk stars) from the upper branch (thick disk stars).

a RC for low extinction sources ($E(B - V) < 0.015$) in DR2.

In Figures 1 and 2 we overplot our RC sample in the bottom panels. The RC stars show a clear NUV-optical color-dependent trend with $[\text{Fe}/\text{H}]$ (higher $[\text{Fe}/\text{H}]$ at redder $(NUV - G)_0$ and vice-versa, shown in Figure 1). This spread is unique to $(NUV - G)_0$ color, especially when the dust correction is applied. In Figure 3 we show the distributions for the RC stars of Galactic longitude, distance, NUV magnitude and $E(B - V)$. The $E(B - V)$ for most of this sample is less than 0.1, suggesting relatively small extinction corrections. Most of the RC sample is between $18 < \text{NUV} < 20$. The GAIS survey limit is 21 (5σ) indicating this sample is reasonably complete out to our distance limit.

Using the derived parameters from APOGEE, we show in Figure 4 that the RC UV-optical color also correlates with effective temperature. The trend for $(G_{BP} - G_{RP})_0$

is much weaker and more highly scattered. From a line fit, we measure $\sigma_{BP-RP_0} = 0.057$ and $\sigma_{NUV-G_0} = 0.23$. Compared to the slope of the RC in each color, the relative scatter is 2.6 times smaller in $(NUV - G)_0$ than in $(G_{BP} - G_{RP})_0$.

4. DISCUSSION

In this section we define an ultraviolet-optical color-metallicity relation. First we separate our RC sample into two subsamples of thin and thick disk stars. Figure 5 shows $[\alpha/\text{Fe}]$ vs $[\text{Fe}/\text{H}]$ and distinguishes between thin and thick disk stars using a simple cut in $[\alpha/\text{Fe}]$ (Hawkins et al. 2015, Nidever et al. 2014). The thick disk stars overall have a much higher $[\alpha/\text{Fe}]$, especially at lower $[\text{Fe}/\text{H}]$. The $[\alpha/\text{Fe}] - [\text{Fe}/\text{H}]$ relation is a unique way to separate different Galactic components to understand the star formation history of different parts of the Milky Way. The thin disk stars are thought to be considerably younger than the thick disk stars because of the smaller amount of α elements (O, Mg, Si, Ca, and Ti) for a given $[\text{Fe}/\text{H}]$. We see the same separation as in Nidever et al. 2014 between the low and high α sequence around $[\text{Fe}/\text{H}] = 0.2$.

The majority of thick disk stars are bluer and very likely hotter than the thin disk subsample. Alternatively, at a given $(NUV - G)_0$, the thick disk stars have a lower $[\text{Fe}/\text{H}]$ than their thin disk counterparts. While none of the thin disk stars are metal poor enough to be considered halo stars (typically metallicities of $[\text{Fe}/\text{H}] < -0.5$), they are not significantly different from the entire sample in other quantities except $[\alpha/\text{Fe}]$. The trends for the two different populations present in Figure 5 suggest different color-metallicity relations between them.

In Figure 6 we show a clear trend between $(NUV - G)_0$ color and metallicity for the full sample that spans a wider range of color than in optical wavelengths as shown in Figure 1. This relation becomes much tighter when an extinction correction is added. We also separate the two thin and thick disk populations in the middle and bottom panels, respectively. We obtain the following relationship for the full extinction-corrected sample:

$$[Fe/H] = 0.256(NUV - G)_0 - 2.204. \quad (1)$$

The standard deviation from the linear fit is $\sigma_{[\text{Fe}/\text{H}]} \sim 0.28$ dex. Equation 1 provides a new means to determine metallicity from photometry with a precision similar to low-resolution spectroscopy (e.g. SDSS SEGUE, Lee et al. 2011, where they measure $[\text{Fe}/\text{H}]$ to a precision of 0.23 dex) but at a much cheaper cost and can be obtained for many more stars.

The two different thin and thick disk populations from Figure 5 appear to have different color-metallicity relations. Thick disk stars have much less scatter from the relation than thin disk stars and the slope is higher in the thick disk color-metallicity relation. At the very metal poor end ($[\text{Fe}/\text{H}] < -0.6$) RC stars appear to be a part of the galaxy's thick disk (Brook et al. 2012, Hawkins et al. 2015) and from Figure 5 they are bluer objects in general. The thin disk population also shows objects that are bluer than expected, including several outliers bluer than $(NUV - G)_0 < 6$, some of which could be binaries. We will leave a more detailed discussion of these outliers to future papers. Even with the presence of outliers, the

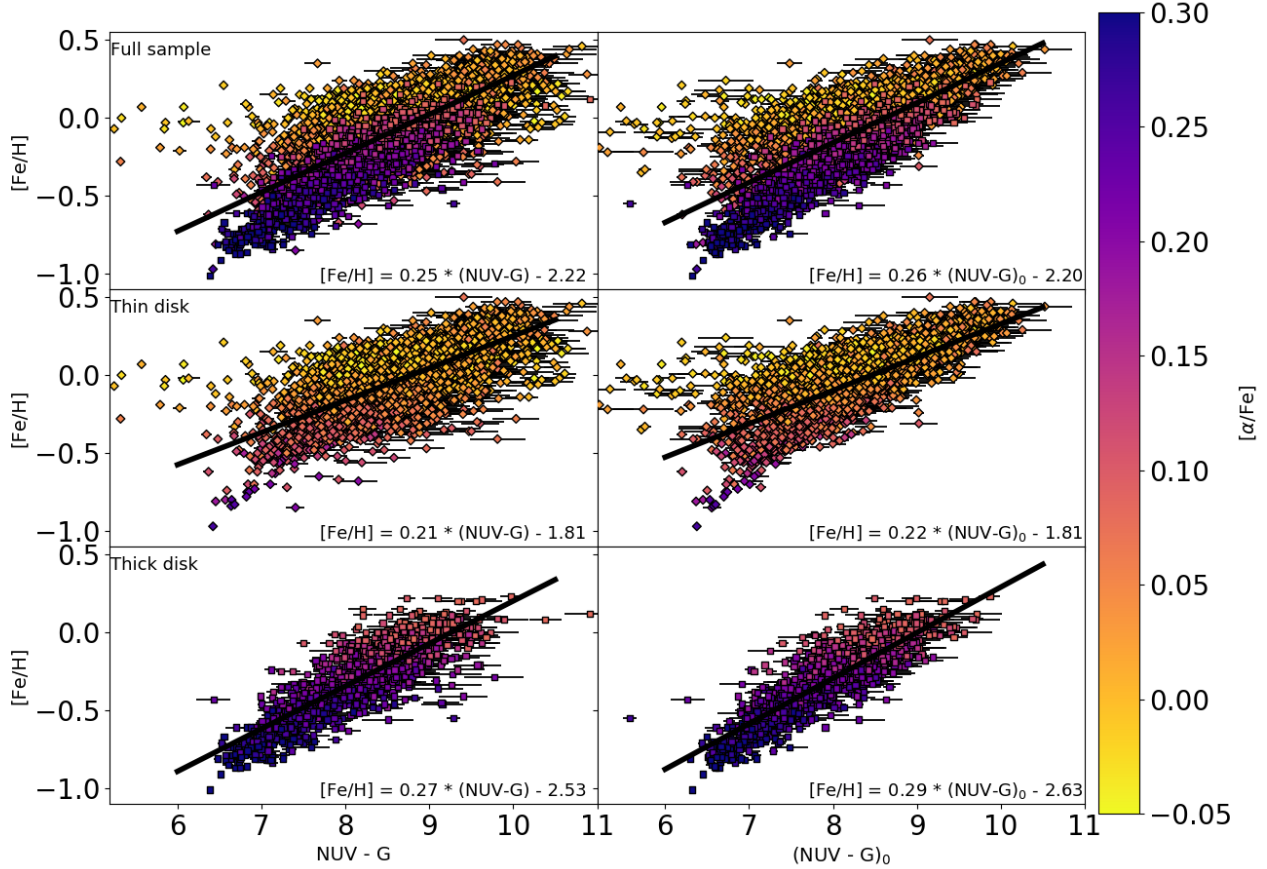


FIG. 6.— $[\text{Fe}/\text{H}]$ vs $(\text{NUV} - G)_0$ colored by $[\alpha/\text{Fe}]$ without (left) and with (right) a Galactic extinction correction. We find several outliers at $(\text{NUV} - G)_0 < 6$ that are possibly binaries. The middle panels show thin disk stars and the bottom panels show thick disk stars. Each fit is done only on the data in that panel. We include all six fits in their corresponding panels. The $(\text{NUV} - G)_0$ spread over 4 magnitudes is much greater than in optical colors. The color-metallicity relation has a weak dependence on $[\alpha/\text{Fe}]$. The trend tightens when corrected for Galactic extinction.

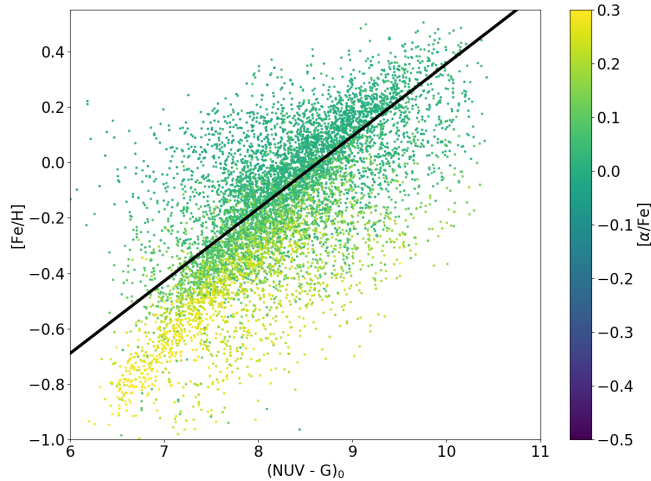


FIG. 7.— $[\text{Fe}/\text{H}]$ vs $(\text{NUV} - G)_0$ for stars within the RC box described in the text. The black line is the dust-corrected fit for the entire sample from figure 6, top right panel. The data match the trend we see at $(\text{NUV} - G)_0 > 7.5$.

overall relation is still about as precise as spectroscopy.

To demonstrate the effectiveness of this color-metallicity relation, we select a subset of photometrically-defined RC stars from the CMD in Figure 1. We define our RC box as bound at $6 > (\text{NUV} - G)_0 > 10.5$ and $0.9 > M_G > -0.1$. This region contains many possible RC candidates from which one can also derive asteroseismic parameters with minimal contamination from RGB stars using the methods in Hawkins et al. 2018. The main sources of bias comes from dust extinction (and uncertainties) in NUV which would restrict the range of objects detectable by GALEX.

We apply the same cuts as described in section 2.2 to a matched catalog between GAIS, Gaia DR2, and APOGEE DR14 and replot the $[\text{Fe}/\text{H}] - (\text{NUV} - G)_0$ relation with these data. The overall trend between ultraviolet-optical color and metallicity closely matches that of the spectroscopically-obtained RC sample. The scatter in the relation is larger but this is likely due to contamination from other giant stars. There is an offset at $(\text{NUV} - G)_0 < 8$ for the highest $[\alpha/\text{Fe}]$ stars which likely is due to the steeper relation for the thick disk stars in this sample.

Photometric-metallicity relations have been calculated

or observed in the past. For example, Ivezić et al. 2008 use F and G main-sequence stars to derive a relation between $[\text{Fe}/\text{H}]$, $u - g$ and $g - r$. The $u - g$ color, or the UV excess, depends on metallicity because of the high absorption of metals at bluer colors, affecting the star’s flux. This UV excess depends on the $g - r$ color which is related to the star’s effective temperature. RC stars are known to have a flux-temperature relation that varies greatly depending on the metallicity. Metal line blanketing may also play a role due to the high $[\text{Fe}/\text{H}]$ values in this sample (Girardi 2016, Choi et al. 2016). Metals in stellar atmospheres absorb blue light due to metal line blanketing and should show significant absorption in bluer wavelengths like NUV. In our sample these metal-rich stars are the reddest, with $(\text{NUV} - G)_0$ values reaching up to 10 magnitudes versus the blue end at $(\text{NUV} - G)_0 = 6$ containing the most metal poor stars (Figure 6). Due to their similarity, these trends may also hold for stars along the giant branch albeit with increased scatter.

Finally we explore how our relation compares to predictions from a recently developed stellar evolutionary code. The MESA Isochrones and Stellar Tracks (MIST) model provides tracks and photometric outputs for a full range of stellar masses and metallicities with sufficient resolution to follow short-lived evolutionary stages (Choi et al. 2016). We used evolutionary tracks for the range of masses and metallicities likely to appear in the Milky Way field RC population, with steps of $[\text{Fe}/\text{H}]$ spaced by 0.25 dex and a uniform distribution of stellar masses. Luminosities were calculated in G, G_{BP} , G_{RP} , and NUV bands, using the most up to date Gaia bandpasses. We applied a photometric selection to the final outputs, selecting stars in a similar region for the RC in the CMD, as described above, while also restricting the model to the core helium-burning phase (MESA EEP 631-707). In Figures 8 and 9 we plot NUV vs $[\text{Fe}/\text{H}]$ colored by T_{eff} and $\log g$, respectively. The extinction-corrected fits for the full sample and thick-disk-only subsample are shown on both plots.

The linear fits in Figure 8 provide a good match to the models over most of the metallicity range of our RC sample. Bluer stars tend to be hotter and have a lower metallicity and vice versa. The fit lines overlap models with the T_{eff} range in Figure 4. Figure 9 shows that our mean fits are consistent with models with $\log g \sim 2.4$, with the thick disk stars having a slightly lower $\log g$ (and T_{eff}) at fixed metallicity. The larger scatter with increasing metallicity in the models is also seen in Figure 6, most notably in the thin disk subsample. This scatter can have many explanations (dust, binaries, star formation history). This topic will be the target of future papers.

RC stars are used as standard candles in infrared due to their constant absolute magnitude and color. Metallicity, mass, age, and extinction make their use as standard candles difficult in bluer wavelengths. Using the color-metallicity relation we can create a metallicity map of the Galaxy (e.g. Önal Taş et al. 2016) and increase the accuracy of RC stars as standard candles. These results also have implications on the use of RC stars as extinction probes (see e.g. Girardi 2016). Yanchulova Merica-Jones et al. 2017 use HST observations that extend to the NUV and explain the spread in color as due to extinc-

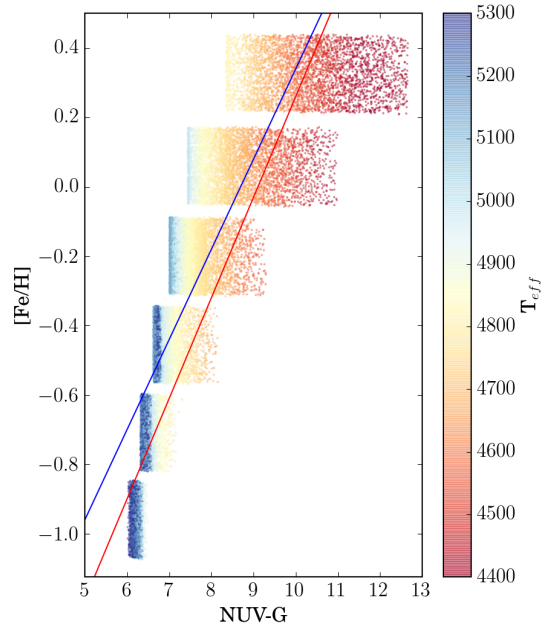


FIG. 8.— Figure 6 plotted with MIST stellar evolution models colored by T_{eff} . The blue line is the fit to the entire sample and the red line is the fit to only the thick disk.

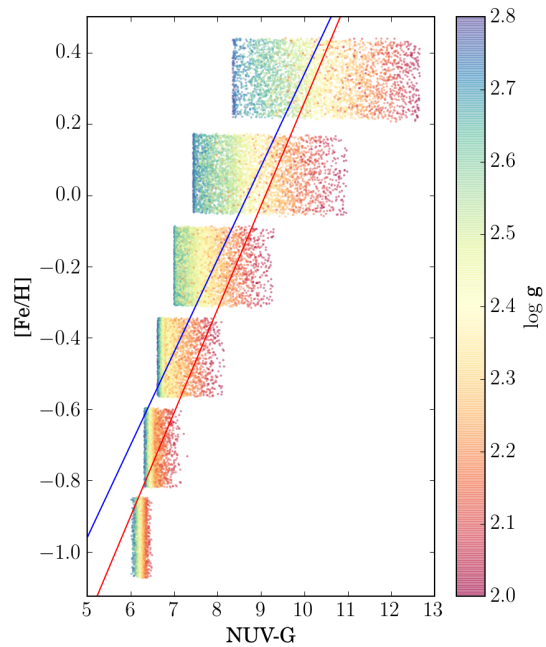


FIG. 9.— Figure 6 plotted with MIST stellar evolution models colored by $\log g$. The blue and red lines are the same as in Figure 8.

tion. They conclude the RC is confined to a small region in the CMD with similar metallicities. We would expect to see a large spread in $(\text{NUV} - G)_0$ over a comparable metallicity range, indicating that metallicity may play a non-trivial role in understanding the RC in CMD space.

5. CONCLUSION

Using a sample of 5,175 RC stars from APOGEE with data from GALEX and Gaia, we identify the RC in UV-optical CMD space as well as the existence of a color-metallicity relation that is tighter in $(\text{NUV} - G)_0$ than

TABLE 1

RA ($^{\circ}$)	Dec ($^{\circ}$)	NUV (mag)	(NUV - G) ₀ (mag)	G _{BP} (mag)	(G _{BP} - G _{RP}) ₀ (mag)	E(B - V) (mag)	DM (mag)	[Fe/H]	T _{eff} (K)	[α /Fe]
0.1300	15.2717	18.11 \pm 0.03	7.46 \pm 0.03	11.17 \pm 0.00	1.16 \pm 0.00	0.04	10.41	-0.41 \pm 0.01	4931.00	0.10 \pm 0.02
0.2081	16.3654	19.40 \pm 0.07	8.82 \pm 0.07	11.18 \pm 0.00	1.31 \pm 0.00	0.04	10.13	0.06 \pm 0.01	4699.00	0.01 \pm 0.01
0.3194	15.3927	19.49 \pm 0.06	9.78 \pm 0.06	10.36 \pm 0.00	1.39 \pm 0.00	0.04	9.10	0.34 \pm 0.01	4553.00	0.02 \pm 0.01
0.4016	0.2359	18.97 \pm 0.04	8.80 \pm 0.04	10.74 \pm 0.00	1.26 \pm 0.00	0.02	9.61	0.04 \pm 0.01	4723.00	-0.01 \pm -0.42
0.5204	15.0377	19.08 \pm 0.05	7.55 \pm 0.05	12.04 \pm 0.00	1.17 \pm 0.00	0.05	11.27	-0.36 \pm 0.01	4915.00	0.13 \pm 0.02
0.6003	16.4273	17.30 \pm 0.02	7.94 \pm 0.02	9.90 \pm 0.00	1.20 \pm 0.00	0.03	9.03	-0.24 \pm 0.01	4826.00	0.03 \pm 0.02
0.6012	16.9140	19.10 \pm 0.06	8.48 \pm 0.06	11.18 \pm 0.00	1.24 \pm 0.00	0.03	10.17	-0.01 \pm 0.01	4782.00	0.03 \pm 0.06
0.6975	17.1347	17.58 \pm 0.03	8.38 \pm 0.03	9.77 \pm 0.00	1.24 \pm 0.00	0.03	9.25	-0.23 \pm 0.01	4734.00	0.02 \pm 0.01
0.9191	16.9788	18.68 \pm 0.05	8.95 \pm 0.05	10.37 \pm 0.00	1.37 \pm 0.00	0.03	9.18	0.17 \pm 0.01	4548.00	0.05 \pm 0.04
0.9634	75.8578	19.44 \pm 0.34	8.37 \pm 0.34	11.79 \pm 0.00	1.53 \pm 0.00	0.30	10.67	0.15 \pm 0.01	4929.00	-0.01 \pm -0.01

NOTE. — (1) Gaia RA, (2) Gaia Dec, (3) GALEX NUV, (4) dust corrected NUV - G, (5) Gaia G_{BP}, (6) dust corrected G_{BP} - G_{RP}, (7) E(B - V) from Green et al. 2015, (8) Distance Modulus, (9) stellar metallicity, (10) the effective temperature from APOGEE \pm 91.47 K for all values, (11) alpha abundance. Table 1 is published in its entirety in the machine-readable format. A portion is shown here for guidance regarding its form and content.

(G_{BP} - G_{RP})₀. We see a strong dependence of color on T_{eff} and metallicity. As part of this analysis, we apply a Galactic extinction correction using a 3-D dust map from Green et al. 2015 and Gaia distances, which further tightens the relation. If we separate the sample into thin and thick disk stars, thick disk stars appear bluer than their thin disk counterparts for a given temperature and redder at a fixed metallicity. Finally, we find a tight relation between (NUV - G)₀ and [Fe/H] with a standard deviation of about $\sigma = 0.28$ that can be used to estimate stellar metallicities of RC stars when a spectroscopic metallicity measurement is missing. This relation will be used to obtain photometric metallicities from other stars in the same CMD space as RC candidates using only their UV-optical color. An NUV GALEX Plane Survey (Mohammed et al., in prep) will provide NUV measurements for the Galactic Plane for the first time using GALEX. This survey will provide millions of new objects brighter than NUV = 20 magnitude that will aid in RC investigations as well as many other fields in Galactic astronomy. Spectroscopic followup of these candidates could confirm their RC status using the method of Hawkins et al. 2018 and Ting et al. 2018 and allow us to further understand

the UV-optical color-metallicity-age relation. RC stars are excellent extinction probes and if their metallicity is known it is enough to use a CMD to fit for its extinction values. Using our color-metallicity relation in conjunction with extinction measurements from Green et al. 2015 we can narrow the variables to mass and age.

We acknowledge support from NASA-ADP Grant NNX12AI50G. GALEX (*Galaxy Evolution Explorer*) is a NASA Small Explorer, launched in 2003 April. This work is based on data from the European Space Agency (ESA) mission Gaia (<https://www.cosmos.esa.int/gaia>), processed by the Gaia Data Processing and Analysis Consortium (DPAC, <https://www.cosmos.esa.int/web/gaia/dpac/consortium>). This study makes use of the publicly released data from APOGEE DR14. This research made use of Astropy, a community-developed core Python package for Astronomy (Astropy Collaboration et al. 2013). We acknowledge Dustin Lang for timely production of the Gaia DR2-GALEX catalog.

REFERENCES

- Astropy Collaboration, Robitaille, T. P., Tollerud, E. J., et al. 2013, *A&A*, 558, A33, doi: 10.1051/0004-6361/201322068
- Brook, C. B., Stinson, G. S., Gibson, B. K., et al. 2012, *MNRAS*, 426, 690, doi: 10.1111/j.1365-2966.2012.21738.x
- Cardelli, J. A., Clayton, G. C., & Mathis, J. S. 1989, *ApJ*, 345, 245, doi: 10.1086/167900
- Choi, J., Dotter, A., Conroy, C., et al. 2016, *ApJ*, 823, 102, doi: 10.3847/0004-637X/823/2/102
- Dotter, A. 2016, *ApJS*, 222, 8, doi: 10.3847/0067-0049/222/1/8
- Gaia Collaboration, Brown, A. G. A., Vallenari, A., et al. 2018a, *ArXiv e-prints*. <https://arxiv.org/abs/1804.09365>
- Gaia Collaboration, Babusiaux, C., van Leeuwen, F., et al. 2018b, *ArXiv e-prints*. <https://arxiv.org/abs/1804.09378>
- García Pérez, A. E., Allende Prieto, C., Holtzman, J. A., et al. 2016, *AJ*, 151, 144, doi: 10.3847/0004-6256/151/6/144
- Girardi, L. 2016, *ARA&A*, 54, 95, doi: 10.1146/annurev-astro-081915-023354
- Green, G. M., Schlafly, E. F., Finkbeiner, D. P., et al. 2015, *ApJ*, 810, 25, doi: 10.1088/0004-637X/810/1/25
- Hawkins, K., Jofré, P., Masseron, T., & Gilmore, G. 2015, *MNRAS*, 453, 758, doi: 10.1093/mnras/stv1586
- Hawkins, K., Leistedt, B., Bovy, J., & Hogg, D. W. 2017, *MNRAS*, 471, 722, doi: 10.1093/mnras/stx1655
- Hawkins, K., Ting, Y.-S., & Walter-Rix, H. 2018, *ApJ*, 853, 20, doi: 10.3847/1538-4357/aaa08a
- Ivezić, Ž., Sesar, B., Jurić, M., et al. 2008, *ApJ*, 684, 287, doi: 10.1086/589678
- Jordi, C., Gebran, M., Carrasco, J. M., et al. 2010, *A&A*, 523, A48, doi: 10.1051/0004-6361/201015441
- Lee, Y. S., Beers, T. C., Allende Prieto, C., et al. 2011, *AJ*, 141, 90, doi: 10.1088/0004-6256/141/3/90
- Lutz, T. E., & Kelker, D. H. 1973, *PASP*, 85, 573, doi: 10.1086/129506
- Majewski, S. R., Schiavon, R. P., Frinchaboy, P. M., et al. 2017, *AJ*, 154, 94, doi: 10.3847/1538-3881/aa784d
- Martin, D. C., Fanson, J., Schiminovich, D., et al. 2005, *ApJ*, 619, L1, doi: 10.1086/426387
- Nidever, D. L., Bovy, J., Bird, J. C., et al. 2014, *ApJ*, 796, 38, doi: 10.1088/0004-637X/796/1/38
- Önal Taş, Ö., Bilir, S., Seabroke, G. M., et al. 2016, *PASA*, 33, e044, doi: 10.1017/pasa.2016.33
- Oudmaijer, R. D., Groenewegen, M. A. T., & Schrijver, H. 1998, *MNRAS*, 294, L41, doi: 10.1046/j.1365-8711.1998.01409.x
- Paxton, B., Bildsten, L., Dotter, A., et al. 2011, *ApJS*, 192, 3, doi: 10.1088/0067-0049/192/1/3
- Paxton, B., Cantiello, M., Arras, P., et al. 2013, *ApJS*, 208, 4, doi: 10.1088/0067-0049/208/1/4

Paxton, B., Marchant, P., Schwab, J., et al. 2015, *ApJS*, 220, 15,
doi: [10.1088/0067-0049/220/1/15](https://doi.org/10.1088/0067-0049/220/1/15)
Ting, Y.-S., Hawkins, K., & Rix, H.-W. 2018, *ApJ*, 858, L7,
doi: [10.3847/2041-8213/aabf8e](https://doi.org/10.3847/2041-8213/aabf8e)
Xiang, M.-S., Liu, X.-W., Yuan, H.-B., et al. 2017, *MNRAS*, 467,
1890, doi: [10.1093/mnras/stx129](https://doi.org/10.1093/mnras/stx129)

Yanchulova Merica-Jones, P., Sandstrom, K. M., Johnson, L. C.,
et al. 2017, *ApJ*, 847, 102, doi: [10.3847/1538-4357/aa8a67](https://doi.org/10.3847/1538-4357/aa8a67)
Yuan, H. B., Liu, X. W., & Xiang, M. S. 2013, *MNRAS*, 430,
2188, doi: [10.1093/mnras/stt039](https://doi.org/10.1093/mnras/stt039)